

INTEGRAL IBIS catalog of magnetar bursts

DOMINIK PATRYK PACHOLSKI ,^{1,2} SANDRO MEREGHETTI ,¹ AND MARTIN TOPINKA ,³

¹INAF, Istituto di Astrofisica Spaziale e Fisica Cosmica di Milano, via Corti 12, I-20133 Milano, Italy

²Università degli Studi di Milano Bicocca, Dipartimento di Fisica G. Occhialini, Piazza della Scienza 3, I-20126 Milano, Italy

³INAF, Osservatorio Astronomico di Cagliari, via della Scienza 5, I-09047 Selargius, Italy

ABSTRACT

One of the distinctive properties of magnetars, young neutron stars powered mainly by magnetic energy, is the emission of short ($\lesssim 1$ s) bursts of hard X-rays. Such bursts have been observed in nearly all the known magnetars, although at different and time-variable rates of occurrence. In the last two decades, the INTEGRAL satellite has extensively covered with good imaging capabilities the Galactic plane, where most magnetars reside. We present the results of a comprehensive search for magnetar bursts in more than twenty years of archival data of the INTEGRAL IBIS instrument (15 keV – 1 MeV). This led to the detection of 1349 bursts with 30–150 keV fluence in the $\sim 2 \times 10^{-9} – 3 \times 10^{-6}$ erg cm $^{-2}$ range from 21 of the 34 examined magnetars and candidate magnetars with well known positions. The durations of the bursts, in terms of T_{90} , follow a lognormal distribution centered at ~ 0.1 s. Most of the detected bursts originated from three particularly active sources: 1E 1547–5408, SGR 1806–20, and SGR 1935+2154. The integral distributions of their burst fluences follow power laws with slopes $\beta = 0.76 \pm 0.04$, 0.95 ± 0.06 , and 0.92 ± 0.10 , respectively. The burst spectra are generally well fit with an exponentially cut-off power law with peak energy E_{peak} in the range $\sim 20 – 60$ keV for SGR 1806–20 and SGR 1935+2154, while the bursts of 1E 1547–5408 are slightly harder ($E_{peak} \sim 35 – 100$ keV). A significant anti-correlation between E_{peak} and fluence is found for SGR 1806–20, which provided the largest number of bursts among the sources of our sample.

1. INTRODUCTION

Magnetars are young, isolated neutron stars with the most extreme magnetic fields, typically in the range of $10^{12} – 10^{15}$ G (C. Kouveliotou et al. 1998; S. Mereghetti et al. 2015; V. M. Kaspi & A. M. Beloborodov 2017). They have spin periods of $\sim 2 – 12$ s and relatively high spin-period derivatives of $10^{-11} – 10^{-13}$ s s $^{-1}$. Unlike rotation-powered pulsars or neutron stars in accreting X-ray binaries, magnetars are believed to be powered by their strong internal magnetic fields (C. Thompson & R. C. Duncan 1996).

Since they are typically faint in their quiescent state, with luminosities of $10^{32} – 10^{35}$ erg s $^{-1}$, many magnetars were first discovered through the detection of short bursts, one of their most defining characteristics (hence the name of “soft gamma-ray repeaters” with which they were initially designated). These bursts, seen mainly in the hard X-ray, are believed to originate in the magnetosphere, triggered by sudden crust failures caused by internal magnetic stresses (C. Thompson & R. C. Duncan 1995, 2001) or by rapid reconfigurations of the magnetic field (M. Lyutikov 2003; R. Gill & J. S. Heyl 2010; K. Parfrey et al. 2013).

Magnetar bursts span a wide range of durations and energies, from a few to several hundred milliseconds, with a mean typically centred around 100 ms, with energies in the range of $10^{39} – 10^{43}$ erg (V. M. Kaspi & A. M. Beloborodov 2017). Their spectra are commonly described by cutoff power-law models or by the sum of two blackbody components (e.g. G. Younes et al. 2017; C. Cai et al. 2022a). In some magnetars that went through several periods of bursting activity, the spectral parameters were observed to evolve (A. von Kienlin et al. 2012; A. C. Collazzi et al. 2015; L. Lin et al. 2020a)

In addition to emitting short bursts (either isolated or grouped in “storms” of tens or hundreds in a short period), magnetars can enter long-term outbursts, during which their persistent emission increases by up to several orders of magnitude (e.g. F. Coti Zelati et al. 2018). These outbursts are often accompanied by active burst periods, with

dozens to hundreds of bursts occurring in rapid succession, as observed in sources such as SGR 1806–20 (D. Götz et al. 2006; G. Younes et al. 2017) and SGR 1935+2154 (e.g. L. Lin et al. 2020b; G. Younes et al. 2020). In contrast, some magnetars have shown little or no bursting activity since their discovery. One example is AX J1818.8–1559, first identified through a single burst detected in 2007 (S. Mereghetti et al. 2012), and with only one possible burst seen eight years later (D. M. Palmer et al. 2015).

Several statistical studies of large samples of magnetar bursts have been published based on data collected with non-imaging instruments on different satellites, including International Cometary explorer (J. G. Laros et al. 1987; A. Ulmer et al. 1993; K. J. Hurley et al. 1994; B. Cheng et al. 1996), Rossi-XTE (E. Göğüş et al. 1999; E. Göğüş et al. 2000, 2001; F. P. Gavriil et al. 2004; Z. Prieskorn & P. Kaaret 2012), KONUS instruments on board of Venera 11–14 (E. P. Mazets & S. V. Golenetskii 1981; R. L. Aptekar et al. 2001), KONUS-Wind (E. P. Mazets et al. 1999), CGRO/BATSE (E. Göğüş et al. 2000; C. Kouveliotou et al. 1994), Fermi/GBM (A. J. van der Horst et al. 2012; L. Lin et al. 2012; A. C. Collazzi et al. 2015), and Insight-HXMT (C. Cai et al. 2022b,a).

Here we report the results of a systematic analysis of magnetar bursts based on data of the INTEGRAL/IBIS instrument, which, thanks to its excellent imaging capabilities in the hard X-ray range, has allowed us to securely identify the magnetar responsible for each detected burst. We used all the public data available up to October of 2024 to detect bursts from all known magnetars and characterise their timing and spectral properties.

2. OBSERVATIONS AND DATA REDUCTION

INTEGRAL is a satellite of the European Space Agency launched in October 2002, which ceased scientific operations in February 2025. It was designed to perform observations over a broad energy range from 3 keV to 10 MeV. This was achieved thanks to three instruments, the Joint European X-Ray Monitor (JEM-X, N. Lund et al. 2003), the Imager on Board the INTEGRAL Satellite (IBIS, P. Ubertini et al. 2003), and the SPectrometer on INTEGRAL (SPI, G. Vedrenne et al. 2003) covering the energy ranges 3–35 keV, 15 keV–1 MeV, and 18 keV – 8 MeV, respectively. INTEGRAL, was able to conduct long and uninterrupted observations, thanks to its highly elliptical orbit with a period of three days until the beginning of 2015 and 64 hours afterwards (E. Kuulkers et al. 2021). Scientific data were acquired during the part of the orbit above the Earth radiation belt ($\sim 40,000$ km, W. Hajdas et al. 2003), i.e. for about 90% of time. All the data were transmitted to Earth in real time, thanks to a continuous telemetry link.

Most of the INTEGRAL observations were performed using a dithering pattern, in order to optimise imaging with the coded mask instruments and to improve background modelling. Each observation was split in individual segments, referred to as Science Windows (ScWs), typically lasting about ~ 30 minutes and pointed on a grid of directions centred around the target source. A large part of the observing time was devoted to a survey of the Galactic plane, again using a predefined pattern of ScWs.

We used data obtained with IBIS, a coded mask telescope with a wide-field of view (FOV) of $29.1^\circ \times 29.4^\circ$ (at zero sensitivity), including a fully coded, most sensitive central part, of $\sim 8^\circ \times 8^\circ$. IBIS is composed of two detectors simultaneously working in different energy ranges: ISGRI (The INTEGRAL Soft Gamma-Ray Imager, F. Lebrun et al. 2003) at lower energies and PICsIT (C. Labanti et al. 2003, Pixellated Imaging Caesium Iodide Telescope) at higher energies. The time resolution and sensitivity of PICsIT are not adequate to study magnetar bursts. Therefore, we only used ISGRI data.

ISGRI is located at 3.2 meters from the IBIS coded mask. The mask is composed of gaps and fully opaque elements of tungsten with a thickness of 16 mm. The mask aperture is based on a Modified Uniformly Redundant Array, an optimal pattern that allows resolution of all sources within the field of view. The images recorded by the ISGRI detector are called shadowgrams, as they are formed by the superposition of mask shadows cast by the sources in the FoV. The analysis of the shadowgrams, through correlation with the mask pattern, enables the reconstruction of the source positions in the sky.

The ISGRI detector is composed of 8 modules of 64×32 CdTe pixels each, with a pixel size of 4×4 mm 2 and spaced by 0.6 mm. Including the spacing between the modules, a total shadowgram has a size of 130×134 pixels and a collecting area of 2600 cm 2 . The detector operates nominally in the 15 keV to 1 MeV range, but the effective area is above 900 cm 2 in the 20 to 100 keV range and drops below 200 cm 2 at $E > 200$ keV. The energy resolution is $\sim 8\%$ at 100 keV (FWHM). ISGRI works in photon-by-photon mode, providing an excellent time resolution of $61\ \mu\text{s}$.

Given the pitch of the detector pixels (4.6 mm), the size of the coded-mask elements (11.2 mm), and the mask distance (3.2 m), the angular resolution of ISGRI is $\sim 12'$ (FWHM). The location accuracy depends on the signal to

noise ratio (SNR). It is typically of ~ 3 arcmin for sources slightly above the detection threshold, but can reach 1.5 arcmin for SNR above 10 (A. Gros et al. 2013).

In the case of bright sources providing a very high count rate, ISGRI data transmission is affected by telemetry saturation. When this occurs, the information on the detected events is not sent to the ground, resulting in gaps in the light curves, typically shorter than a second. For a few bursts affected by this problem, we implemented a correction by linearly interpolating the count rates between saturated periods. In these cases, the estimated flux and fluence are indicated as lower limits in the following figures and tables.

As a result of radiation damage in the CdTe pixels, ISGRI experienced a gain decrease of $\sim 2.6\%$ per year, which was within the expectations (F. Lebrun 2005). In addition, up to 1% gain drop was also caused by strong solar flares (see IBIS Observer's Manual⁴). As a result, the low threshold of the energy range suitable for spectral analysis evolved with time, reaching a value of 25 keV in 2014, and then almost 40 keV at the end of the mission. Some of the detector pixels can produce spurious events caused by electronic noise, which are flagged and subsequently filtered out in the analysis (only events with "SELECT_FLAG" equal to 0 are used).

The source count rates measured by the detector must be corrected for dead time effects. We computed the dead time correction including also the effects induced by the Veto system, by the photons of the on-board calibration source, and (if enabled) by the tagging of Compton events⁵. These three effects cause a dead time ϵ_{hk} which can be computed from the housekeeping data of each ScW. The true count rate can then be expressed as: $N_{true} = N_{rec} \cdot \tau_{tot}$, with τ_{tot} given by:

$$\tau_{tot} = \exp \left(\epsilon_{hk} + \frac{N_{rec}}{M} \tau \right) \quad (1)$$

where $\tau = 0.114$ ms is the fixed dead time during which a pixel cannot register a new event and M is the number of modules illuminated by the source for at least 20% of their surface.

The sources in the partially coded field of view do not illuminate the whole detection plane. Therefore, their observed count rate must be corrected for the coding fraction (COD), i.e., the fraction of the detector area exposed to the source. In the following, all reported numbers of burst counts refer to these corrected values unless stated otherwise.

3. DATA ANALYSIS

3.1. Burst Search

We considered the 34 sources listed in Table 1. Besides the confirmed magnetars, this sample also includes the two rotation-powered pulsars that exhibited magnetar-like emission, PSR J1119-6127 (R. F. Archibald et al. 2016; E. Göğüş et al. 2016) and PSR J1846-0258 (F. P. Gavriil et al. 2008; H. Blumer et al. 2021; R. Sathyaprakash et al. 2024). For each of the considered sources, we selected all the public ScWs (available at 2024 September 30) pointed within 14.5° from the source position. All the ScWs were screened to remove those affected by variable background. This was done by fitting a constant to the light-curve of the whole detector in the full energy range binned at one second, after performing sigma-clipping to exclude possible bursts. ScWs were considered to have good quality and used in the search for bursts if they had $\chi_r^2 \leq 1.3$. This selection resulted in the exclusion of $\sim 8\%$ ScWs per source on average.

The Pixel Illumination Factor (PIF) describes the fraction of pixel area illuminated by a source. Applying a threshold on PIF values allows one to reduce the number of background events and thus to increase the sensitivity of the search. Before the search, the position of the source was considered to create the PIF matrix for each ScW and filter the list of events with it. In particular, we extracted the source light curves using only pixels with $PIF > 0.5$.

The burst search was then performed on the selected ScWs using the following procedure. The search was done in eight time intervals with logarithmically spaced durations between 0.01 and 1.28 s. The threshold for each timescale was set at a level above the average (estimated from the sigma-clipped background level in the 1-second light source curve) corresponding to a false positive probability of 10^{-3} for each ScW. We used the nominal 15-150 keV energy range in all the ScWs.

Typically, a single variability event can exceed the thresholds in several timescales and/or bins. After joining adjacent bins, only the trigger with the highest significance was retained.

The triggers found in the light curves were then verified by making images of the corresponding time intervals. This was done with an interactive analysis based on the imaging software developed for the INTEGRAL Burst Alert

⁴ integral.esac.esa.int/AO21/IBIS_ObsMan.pdf

⁵ Events producing a coincident signal both in ISGRI and in PICsIt

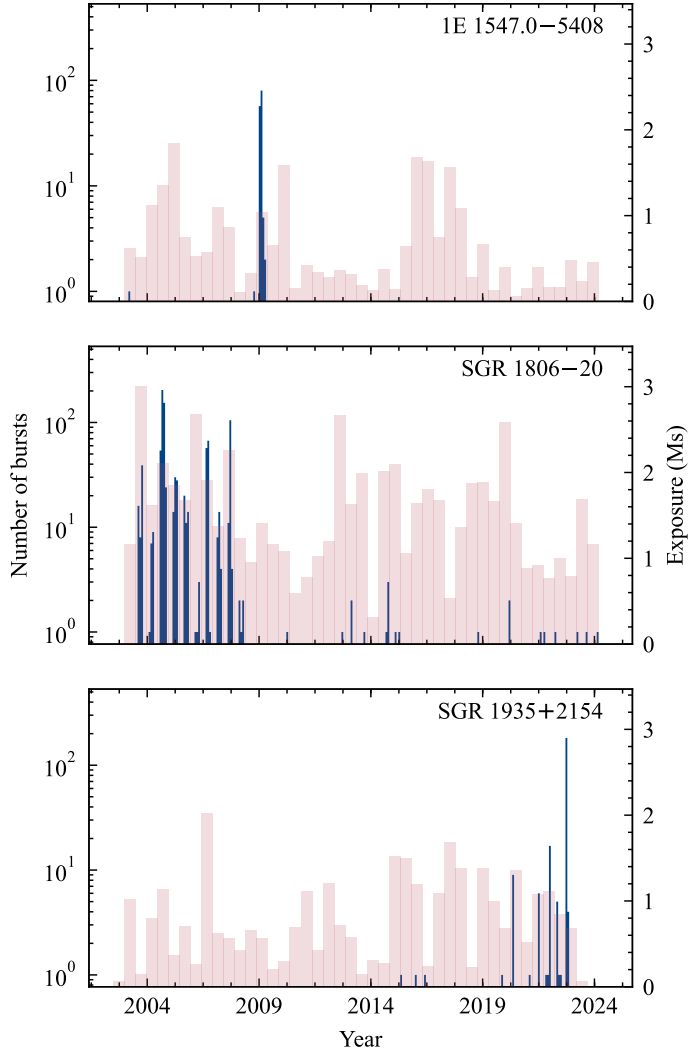


Figure 1. Time distribution of the bursts (blue histograms) and exposure time (red histograms) of 1E 1547–5408 (upper), SGR 1806–20 (middle), and SGR 1935+2154 (bottom). The bursts are in bins of 30 days, while the exposure is for bins of 180 days.

System (IBAS, [S. Mereghetti et al. 2003](#)). This allowed us to eliminate triggers caused by background variations, sources outside the field of view, or coming from other sources in the field of view but unrelated to the magnetar of interest.

In this way, 1349 magnetar bursts were confirmed among more than 75,000 potential triggers found in the light curves search. A summary of the number of bursts and analysed exposure time for each source is provided in Table 1. The largest number of bursts originated from SGR 1806–20, followed by 1E 1547–5408, and SGR 1935+2154. The time distributions of the bursts from these three sources are shown in Fig 1, where we also indicate the analysed exposure time. Additionally, 37 bursts were detected from 18 other magnetars.

In Table 2⁶ we give the unique number identifier for each burst, the timing information (see below), the coding fraction (COD), and the fluences in counts (background-subtracted and corrected for the coding fraction).

3.2. Timing Analysis

The timing characterisation of the bursts was performed using the Bayesian Blocks (BB) method ([J. D. Scargle 1998; J. D. Scargle et al. 2013](#)), in particular to estimate their duration and to define the time intervals for the spectral analysis. This is a non-parametric technique that characterises intensity variations from an unbinned list of event

⁶ Only the first lines are given here; the whole table is available in the electronic version.

Table 1. List of the magnetars with coordinates, exposure time and number of detected bursts.

Source	R.A.	Dec.	Exposure	Bursts
			(J2000)	(Ms)
CXO 0100-7211	01:00:43	-72:11:34	7.96	1
4U 0142+614	01:46:22	61:45:03	21.35	0
SGR 0418+5729	04:18:34	57:32:23	8.90	0
4XMM J045626.3-694723	04:56:26	-69:47:23	14.15	0
SGR 0501+4516	05:01:07	45:16:34	9.21	8
SGR 0525-66	05:26:01	-66:04:36	11.94	2
SGR 0755-2933	07:55:43	-29:33:49	9.55	0
1E 1048-5937	10:50:07	-59:53:21	23.75	2
PSR J1119-6127	11:19:14	-61:27:49	25.13	1
1E 1547.0-5408	15:50:54	-54:18:24	27.09	146
Swift J1555.2-5402	15:55:09	-54:03:41	27.43	0
PSR J1622-4950	16:22:45	-49:50:53	28.55	0
SGR 1627-41	16:35:52	-47:35:23	29.04	2
CXOU J164710-455216	16:47:10	-45:52:17	31.60	3
1RXS J170849-400910	17:08:47	-40:08:52	61.82	2
CXOU J171405-381031	17:14:06	-38:10:31	66.88	1
SGR J1745-2900	17:45:40	-29:00:30	67.93	0
SGR 1801-23	18:00:59	-22:56:49	67.04	2
SGR 1806-20	18:08:39	-20:24:40	65.23	934
XTE J1810-197	18:09:51	-19:43:52	64.44	3
Swift J1818.0-1607	18:18:04	-16:07:32	52.89	1
AX J1818.8-1559	18:18:51	-15:59:23	52.12	1
Swift J1822.3-1606	18:22:18	-16:04:27	52.20	1
SGR J1830-0645	18:30:42	-06:45:17	25.28	0
SGR 1833-0832	18:33:44	-08:31:08	25.50	3
Swift J1834.9-0846	18:34:52	-08:45:56	25.62	0
1E 1841-045	18:41:19	-04:56:11	28.21	1
AX J1845.0-0258	18:44:55	-02:56:53	30.51	0
PSR J1846-0258	18:46:25	-02:58:30	30.57	2
3XMM J185246.6+003317	18:52:47	00:33:18	31.18	0
SGR 1900+14	19:07:14	09:19:20	27.57	1
SGR 1935+2154	19:34:56	21:53:48	32.90	232
SGR 2013+34	20:13:57	34:19:48	27.98	0
1E 2259+586	23:01:08	58:52:45	25.24	0

arrival times by dividing the data into blocks, each of which shows no statistically significant variations in count rate. This ensures that each block is consistent with a period of stable intensity. Only statistically significant changing points are introduced, based on a parameter, p_0 , that represents the false-positive probability threshold used to determine the change points in the data. The BB analysis was done on a 30 s long time interval centered on each burst and we used $p_0=0.05$.

To allow comparison with results in the literature, we also computed the bursts T_{90} , which is the duration of the time interval containing 90% of the burst fluence (setting T_{start} and T_{stop} at times corresponding to 5% and 95% percent of the counts, respectively). The background level for the T_{90} computation was derived from the BB results.

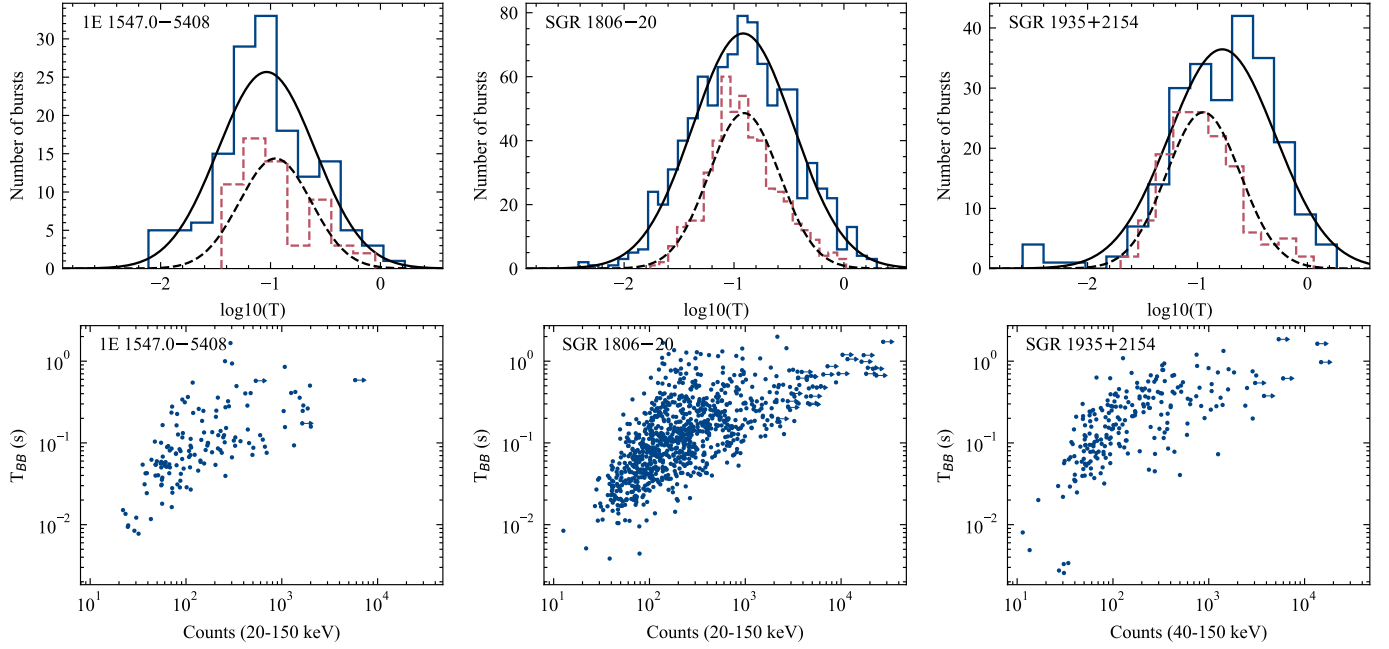


Figure 2. Top panels: Distributions of the burst durations fitted with lognormal functions for 1E 1547–5408 (left), SGR 1806–20 (middle), and SGR 1935+2154 (right). Solid lines refer to T_{BB} and dashed lines to T_{90} . Bottom panels: T_{BB} duration as a function of the number of counts for the same three magnetars.

In particular, we selected the two blocks with the longest duration, one before and one after the burst, and took their average as the background count rate. The background-subtracted integral distribution of burst counts was then fitted with an error function plus a linear term to take into account residual background fluctuations that were present in some cases. However, this method had limitations, particularly when dealing with very faint bursts or certain burst shapes, which prevented a correct fit, usually causing unnaturally large T_{90} . Thus, each burst light curve was visually inspected and rejected in case of incorrect estimation. T_{90} could be estimated for 692 bursts. No alternative T_{90} estimation methods were applied to the problematic cases, to maintain consistency throughout the analysis.

3.3. Spectral analysis

We performed a spectral analysis for the bursts with at least 100 observed counts in the 20–150 keV range for bursts before January 2018, or in the 40–150 keV range after this date. For the spectral analysis, we used the pyXspec (C. Gordon & K. Arnaud 2021) version 2.1.4 with the Xspec version 12.14.1 (K. A. Arnaud 1996). Burst spectra were extracted using the standard pipeline with OSA 11.2 (A. Goldwurm et al. 2003) using custom-defined Good Time Intervals (GTI) that were based on the T_{BB} durations of the bursts. If a burst was affected by telemetry saturation, the saturated periods were excluded from the GTIs. The energy range E_{min} – E_{max} used for the spectral analysis depended on the date of the burst, in order to take into account the evolution of the lower energy threshold. We used E_{min} values between 20 and 32 keV, depending on the observation date, and $E_{max} = 300$ keV. The energy range was divided in 16 or in 13 logarithmic channels. The spectra were rebinned to obtain a minimum of 20 counts in each bin, and 5% systematic errors were added to the data. We considered two models, a simple power law and a power law with exponential cut-off (often called Comptonized model in the literature), defined as follows:

- power law (PL): $F(E) = kE^\alpha \text{ ph cm}^{-2} \text{ s}^{-1} \text{ keV}^{-1}$,
- cut-off power law (CPL): $F(E) = kE^\alpha \exp(-(E(2 + \alpha)/E_{peak})) \text{ ph cm}^{-2} \text{ s}^{-1} \text{ keV}^{-1}$.

For the bursts with the highest number of counts we performed also a time-resolved analysis by extracting spectra from different time intervals (only bursts from SGR 1806–20 and SGR 1935+2154 satisfied this requirement). The analysis was done as described above, using the 20–300 keV and 32–300 keV energy ranges, for SGR 1806–20 and SGR 1935+2154, respectively, divided in 13 bins.

The selection of the burst segments was based on the Bayesian Blocks; however, in some cases, the segmentation was done manually only based on the visual inspection of the light curve and Bayesian block structure. If the block

Table 2. Detected bursts from magnetars.

No	Source	T_{start} (UTC)	T_{BB} (ms)	T_{90} (ms)	COD	CTS_{20-40}	CTS_{40-100}	$CTS_{100-150}$
0	1E 1547.0-5408	2003-03-14 00:09:42.553	68.0	...	0.74	1.7	39.0	16.5
1	SGR 1627-41	2003-03-25 02:45:59.024	111.7	...	1.00	0.0	27.0	19.7
2	1RXS J170849-400910	2003-03-26 05:48:55.080	121.9	...	0.98	4.3	33.3	18.3
3	SGR 1833-0832	2003-04-26 11:34:19.751	532.9	...	0.67	26.8	50.6	9.1
4	1E 1048-5937	2003-07-04 01:53:56.652	2303.3	142.3	1.00	33.5	70.8	18.2
5	SGR 1806-20	2003-08-23 17:32:11.718	216.1	121.8	0.10	104.0	190.8	29.8
6	SGR 1806-20	2003-08-23 22:05:01.450	129.5	91.3	0.40	171.2	138.1	4.8
7	SGR 1806-20	2003-08-23 22:05:01.776	87.6	...	0.40	85.5	97.6	10.1
8	SGR 1806-20	2003-08-24 15:01:11.846	213.0	189.9	0.86	48.4	55.7	11.8
9	SGR 1806-20	2003-08-24 15:30:44.152	254.8	177.2	0.86	240.0	172.6	19.8

NOTE—The whole table is available online in machine-readable format. A portion is shown here for guidance regarding its form and content.

Table 3. Properties of the burst durations.

Source		Average (ms)	10^μ (ms)	σ
1E 1547-5408	T_{BB}	157.3	92.5 ± 7.8	0.44 ± 0.03
	T_{90}	154.4	110.2 ± 10.6	0.32 ± 0.03
SGR 1806-20	T_{BB}	206.6	120.7 ± 4.2	0.46 ± 0.01
	T_{90}	165.9	123.4 ± 4.2	0.32 ± 0.01
SGR 1935+2154	T_{BB}	274.0	168.5 ± 12.3	0.48 ± 0.02
	T_{90}	159.1	113.1 ± 7.5	0.33 ± 0.02

NOTE— μ and σ are the mean and standard deviation of lognormal fits to the distributions of durations.

contained sufficient counts, it was divided into segments of approximately equal duration; conversely, adjacent blocks were merged when individual segments lacked sufficient statistics.

4. RESULTS

4.1. Burst durations

The derived durations of all the bursts are given in Table 2 and the distributions of T_{BB} and T_{90} for SGR 1806-20, 1E 1547-5408, and SGR 1935+2154 are shown in the top panels of Fig. 2. The bottom panels of the same figure show the duration T_{BB} as a function of the number of counts. The distributions of both T_{BB} and T_{90} are well fit with log-normal curves⁷, as also confirmed using the Kolmogorov-Smirnov test. The burst average durations and the best fit parameters of the log-normal fits (mean μ and standard deviation σ) for the three sources are given in Table 3.

As it is shown in Fig. 3, T_{BB} is generally longer than T_{90} . Indeed, T_{BB} is an estimate of the whole burst duration and the BB algorithm is more sensitive to measure faint emission extending before and/or after the main burst peaks. The durations estimated with T_{BB} suggest a tendency for shorter bursts in 1E 1547-5408 and longer ones in SGR

⁷ Two particularly long bursts emitted by SGR 1806-20 on 2004 October 5 (n.387 and n.414) have been excluded from this analysis, because they were affected by telemetry saturation and most likely involved the superposition of several bursts. They have been analysed in detail by D. Götz et al. (2006).

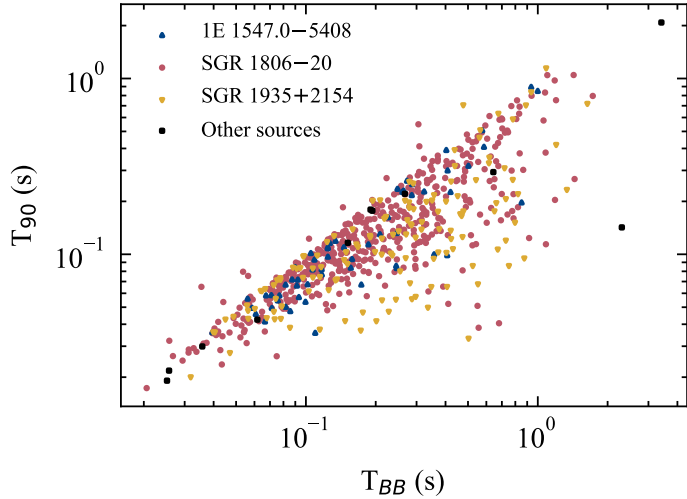


Figure 3. T_{90} versus T_{BB} of all the bursts for which T_{90} could be estimated.

Table 4. Results of the timed-averaged spectral analysis of the bursts.

No	Source	Power law			Cutoff power law			
		α	$\chi^2_r(\text{dof})$	Flux	α	E_{peak}	$\chi^2_r(\text{dof})$	
				$(10^{-7} \text{ erg cm}^{-2} \text{ s}^{-1})$		(keV)		
6	SGR 1806-20	-2.2 ± 0.2	1.6(8)	2.9 ± 0.4	$-0.5^{+1.3}_{-1.0}$	$46.3^{+8.6}_{-9.6}$	1.3(7)	$3.0^{+0.4}_{-0.5}$
9	SGR 1806-20	$-0.4^{+1.0}_{-0.9}$	$40.0^{+5.2}_{-8.8}$	1.5(6)	1.6 ± 0.2
14	SGR 1806-20	-2.1 ± 0.3	0.8(6)	3.3 ± 0.6
17	SGR 1806-20	-2.1 ± 0.2	0.8(9)	1.6 ± 0.2
19	SGR 1806-20	-2.1 ± 0.1	0.8(9)	2.1 ± 0.2
28	SGR 1806-20	-2.6 ± 0.1	1.5(8)	4.4 ± 0.4
32	SGR 1806-20	$-0.6^{+0.5}_{-0.9}$	$24.9^{+3.2}_{-10.8}$	0.6(8)	12.0 ± 0.8
34	SGR 1806-20	-2.8 ± 0.2	1.4(7)	2.2 ± 0.3
35	SGR 1806-20	-2.4 ± 0.2	1.3(7)	1.1 ± 0.2
36	SGR 1806-20	$-2.1^{+0.3}_{-0.4}$	0.7(4)	1.3 ± 0.3

NOTE—The whole table is available online in machine-readable format. A portion is shown here for guidance regarding its form and content.

1935+2154. On the other hand the parameters of the T_{90} distributions are very similar for the three sources. This apparent discrepancy is probably due to the limitations in deriving reliable T_{90} described in section 3.2. In fact T_{90} could not be measured for the faintest bursts, therefore a direct comparison between the average T_{90} and T_{BB} is not straightforward because they refer to different samples.

4.2. Burst spectra

In total, 535 bursts had enough counts for spectral analysis. The results of the spectral fits for each burst are listed in Table 4. The power law model provided an acceptable fit for 313 bursts, while a CPL was required in 114 cases. The other bursts could not be well fitted with either model (due to saturation problems or because the fit parameters were completely unconstrained). For 54 of the bursts adequately fit by a PL, the addition of a cut-off provided a statistically significant improvement, as determined by an F-test with a p-value below 0.15. Thus, in summary, we have a sample of 168 bursts for which α and E_{peak} could be derived, although for some of them (30), the peak energy E_{peak} was poorly constrained (the lower bound of its confidence interval was below 10 keV).

Table 5. Average spectral parameters and Energy Conversion Factors for the cut off power law model.

Source	α_{PO}	α_{CPL}	E_{peak}^a	ECF_{20-150}^b	ECF_{40-150}^c
1E 1547–5408	-1.78 ± 0.03	-0.32 ± 0.11	43.3 ± 0.7	1.1	2.2
SGR 1806–20	-2.42 ± 0.01	-0.60 ± 0.07	32.4 ± 0.4	0.9	2.2
SGR 1935+2154	-2.68 ± 0.03	0.03 ± 0.25	37.7 ± 1.4	...	1.9

^akeV

^bfrom counts in the 20 – 150 keV range to 10^{-10} erg cm $^{-2}$ in the 30 – 150 keV range.

^cfrom counts in the 40 – 150 keV range to 10^{-10} erg cm $^{-2}$ in the 30 – 150 keV range.

We computed the error-weighted average values of the best fit spectral parameters. The average values of the CPL model were then used to estimate Energy Conversion Factors (ECFs) from the count rates (20 – 150 keV and 40 – 150 keV) to the 30 – 150 keV flux in physical units. The average spectral parameters and the ECFs are listed in Table 5. The relation between α and E_{peak} is plotted in the top panels of Fig. 4, while the bottom panels of the same figure show how the spectral parameters depend on the burst fluence.

These figures show evidence for some correlations between the parameters. To quantify this taking into account the measurement errors, we computed the Spearman’s rank correlation coefficient ρ with a Monte Carlo approach that combines bootstrap resampling with perturbations (P. A. Curran 2014) drawn from the split-normal error distributions for each data point. We found a very significant anti-correlation between E_{peak} and fluence for SGR 1806–20, with a mean $\rho = -0.48 \pm 0.07$ and a mean z -score of 7.1 ± 1.0 from 100,000 Monte Carlo tests. For this source, there is also marginal evidence for a correlation between α and E_{peak} ($\rho = -0.31 \pm 0.09$, z -score=3.4±1.1). These correlations are less significant for the other two magnetars (see the ρ and z -score values in Table 6).

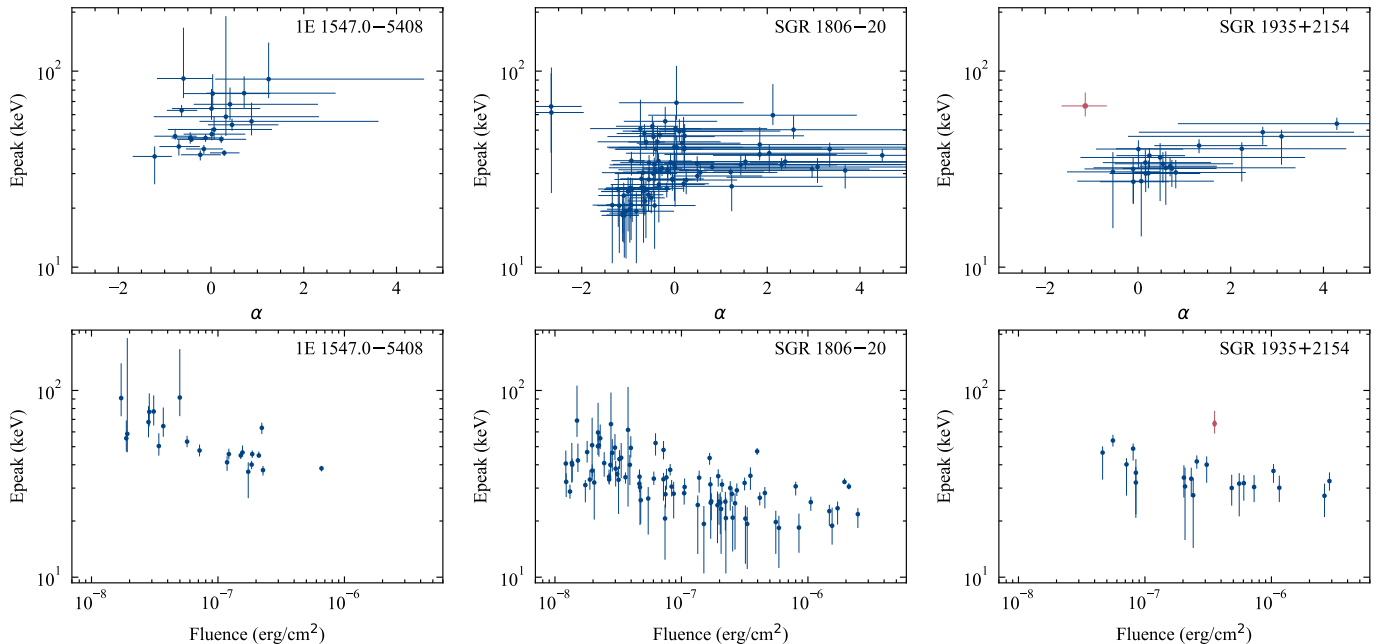


Figure 4. E_{peak} versus α (upper panels) and versus fluence (bottom panels) for the spectra fitted by the cut-off power law model. The figure show results for three sources: 1E 1547–5408 (left), SGR 1806–20 (middle), and SGR 1935+2154 (right). The fluence refers to the 30–150 keV range. The 2020 April 28 burst from SGR 1935+2154 with associated FRB-like emission is indicated in red.

Table 6. Spearman’s rank correlations and best fit parameters of the fluence distributions ($N(>S) \propto S^{-\beta}$, for $S > S_{min}$)

Source	$\rho(E_p, S)$	z -score	$\rho(E_p, \alpha)$	z -score	β	S_{min}
						$(10^{-8} \text{ erg cm}^{-2})$
1E 1547–5408	-0.51 ± 0.19	2.5 ± 1.2	0.22 ± 0.19	1.0 ± 1.1	0.76 ± 0.04	0.53
SGR 1806–20	-0.48 ± 0.07	7.1 ± 1.0	0.31 ± 0.09	3.4 ± 1.1	0.95 ± 0.06	1.89
SGR 1935+2154	-0.39 ± 0.15	2.2 ± 0.9	0.38 ± 0.17	2.1 ± 1.1	0.92 ± 0.10	3.95
SGR 1935+2154 ^a	-0.45 ± 0.15	2.5 ± 1.0	0.46 ± 0.16	2.6 ± 1.1

^aExcluding burst coincident with FRB 200428

We performed time-resolved spectral analysis for 21 bursts (15 from SGR 1935+2154 and 6 from SGR 1806–20). First we fitted the spectra with the power law model and no significant spectral evolution was observed in the photon index. Therefore, we then used the cutoff power law model, keeping α tied across all the time intervals of each burst, while E_{peak} and the normalization were allowed to vary independently.

In the majority of cases, E_{peak} was found to be consistent, within the errors, with a constant value. Only in five cases, we detected a marginally significant variation (p-value < 0.05 , for bursts no 193, 1118, 1244, and 1310 and p-value < 0.1 for no 1260). These are shown in Fig. 5 and their spectral parameters are given in Table 7.

4.3. $\log N - \log S$

For each of the three magnetars with a large number of detected bursts we calculated the integral distribution of burst fluences. The fluences, S , in the 30–150 keV energy range were computed from the number of counts using the ECF values reported in Tab. 5. These distributions (LogN-LogS) are plotted in Fig. 6. In order to compare these distributions with other published results, we fitted them with a power law model ($N(>S) \propto S^{-\beta}$). To avoid potential biases resulting from least-square fitting of the binned differential distributions, we followed a maximum-likelihood approach to derive from the unbinned data the power law slope β and the minimum fluence S_{min} above which a power-law is a good description of the data (D. F. Crawford et al. 1970; A. Clauset et al. 2009). The results obtained for the three sources are given in Table 6. The deviation from a power-law trend visible at low fluences is due to the decreasing efficiency in the detection of the faintest bursts. In fact the highest S_{min} value was obtained for SGR 1935+2154, that was active during the latest part of the mission, when the ISGRI sensitivity decreased.

5. DISCUSSION

5.1. 1E 1547–5408

The active period of 1E 1547–5408 spanned from October 2008 to April 2009 and included three distinct bursting episodes (e.g. P. Scholz & V. M. Kaspi 2011; A. J. van der Horst et al. 2012), in which INTEGRAL detected 1, 106, and 38 bursts, respectively. V. Savchenko et al. (2010) studied the January 2009 activity using both the Anti-Coincidence Shield (ACS) of the spectrometer and ISGRI, reporting over 200 bursts with ACS and 84 with ISGRI. They measured a burst duration distribution centred at 68 ± 3 ms using ACS data. In comparison, our ISGRI analysis during the same period yielded a longer duration distribution. Although discovered several years earlier, 1E 1547–5408 was suggested as a magnetar candidate only in 2007, based on its association with SNR G327.24–0.13 and the discovery of radio pulsations (J. D. Gelfand & B. M. Gaensler 2007; F. Camilo et al. 2007). The first bursts from this source were reported by Swift during the 2008 October outburst (P. Scholz & V. M. Kaspi 2011), but a burst detected by INTEGRAL on 14 March 2003 (no 0 in Table 2) indicates that 1E 1547–5408 was also active at earlier times. A. von Kienlin et al. (2012) reported spectral evolution between the first and third active periods. In our case, such evolution, between the second and the third period, could not be assessed due to the limited number of bursts with sufficient counts for detailed spectral fitting during the third period, as only two bursts could be fitted with the cut-off power-law model. The fluence distribution of 1E 1547–5408 bursts was previously derived using Swift/XRT data in the 1–10 keV range by P. Scholz & V. M. Kaspi (2011), who found a power law index $\beta = 0.6 \pm 0.1$. A similar slope was obtained at higher energies (8–200 keV, $\beta = 0.7 \pm 0.2$) with the Fermi/GBM instrument (A. J. van der Horst et al. 2012) and with the

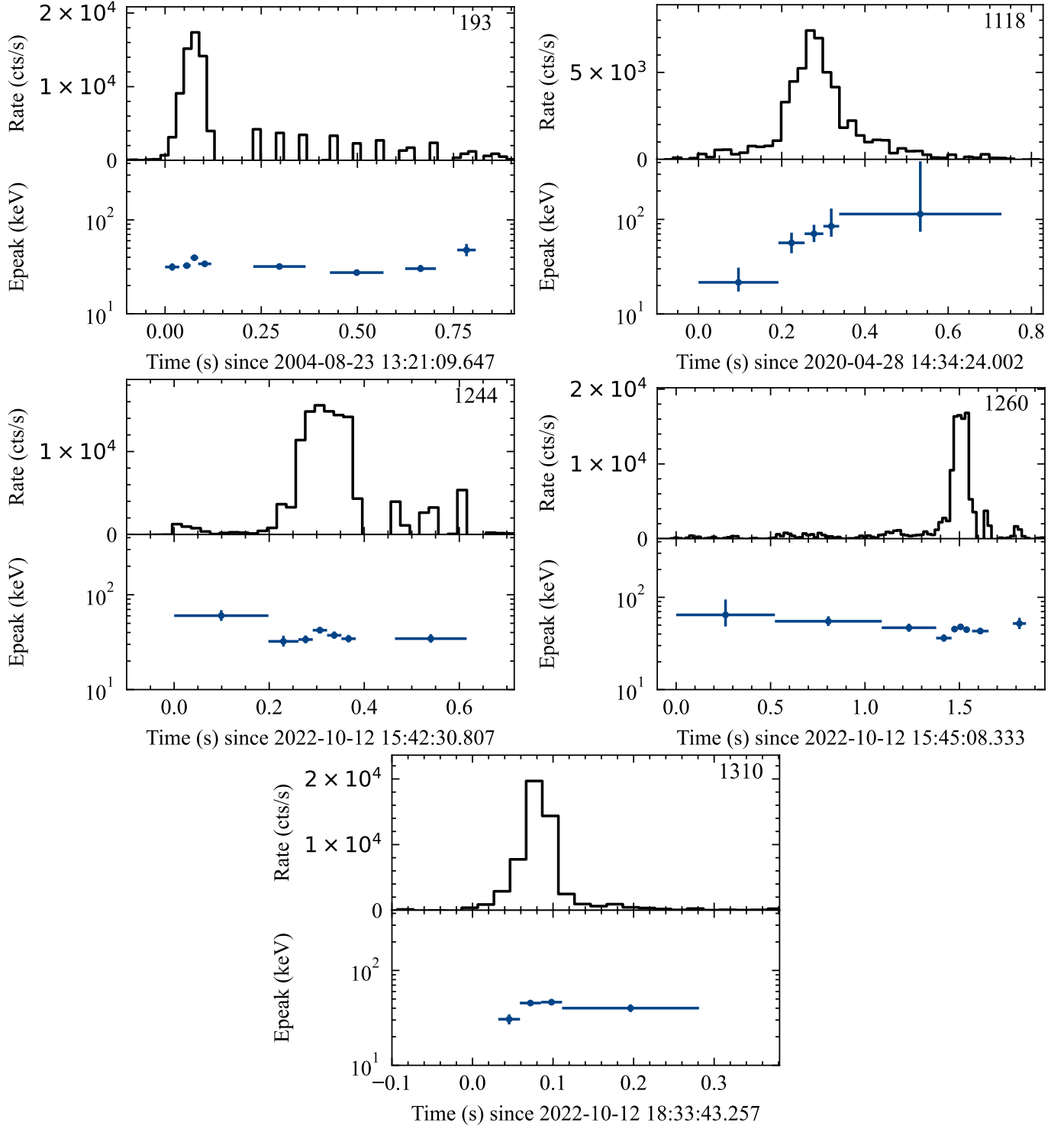


Figure 5. Time resolved spectral analysis of one burst (n. 193) from SGR 1806–20 and four bursts from SGR 1935+2154. The upper panel in each figure shows the background subtracted light curve of the burst, while the bottom panel shows the time evolution of E_{peak} . The gaps in the light curve of burst n. 193 are due to telemetry saturation.

INTEGRAL SPI/ACS instrument at $E > 80$ keV ($\beta = 0.75 \pm 0.06$, S. Mereghetti et al. (2009)). All these results are in agreement with the value $\beta = 0.76 \pm 0.05$ derived in our analysis.

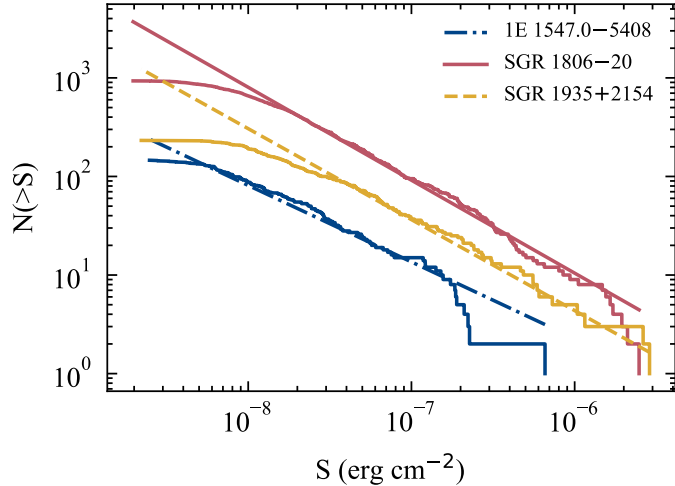


Figure 6. LogN-LogS distributions of bursts of 1E 1547–5408 (grey), SGR 1806–20 (yellow), and SGR 1935+2154 (blue). The best fit power laws are indicated by the dashed lines. The fluence S refers to the 30–150 keV energy range.

The 1E 1547–5408 bursts detected by IBIS are on average harder than those seen from the other two magnetars (see Fig. 4 and Table 5). We obtained an average value of $E_{peak} = 43.7 \pm 0.7$ keV consistent with that obtained with Fermi/GBM during the January 2009 activity period (L. Lin et al. 2012), which is the one that dominates our sample (see Fig. 1).

5.2. SGR 1806–20

SGR 1806–20 was the most active source during the INTEGRAL mission, with a total of 934 bursts and, providing the largest sample in our data, it dominates the overall burst statistics. The bursting activity of SGR 1806–20 began with a high-bursting period over a year before the Giant Flare in 2004 (S. Mereghetti et al. 2005). After April 2008 only 20 bursts were detected in our data, and also other satellites detected only sporadic bursts (A. C. Collazzi et al. 2015; G. Younes et al. 2017). The fluence distribution of the bursts detected from SGR 1806–20 follows a power law of slope 0.95 ± 0.06 for fluences above $\sim 2 \times 10^{-8}$ erg cm $^{-2}$. This agrees well with the previous value, $\beta = 0.91 \pm 0.09$, obtained with a smaller subset of these bursts (D. Götz et al. 2006). Flatter slopes ($\beta \sim 0.5$) were found for the bursts detected with the *RXTE* satellite (Z. Prieskorn & P. Kaaret 2012; E. Göögüs et al. 2000), which operated at lower energies (2–60 keV).

5.3. SGR 1935+2154

All the bursts detected for SGR 1935+2154 occurred between 2015 and 2022. This sample includes the burst with associated FRB-like radio emission on 2020 April 28 (S. Mereghetti et al. 2020; CHIME/FRB Collaboration et al. 2020; C. D. Bochenek et al. 2020), but the period of high bursting activity that preceded this event (G. Younes et al. 2020; Y. Kaneko et al. 2021) was not observed by INTEGRAL. Most of the bursts were detected during the outburst of October 2022 (186 bursts between October 10 and 16). This outburst was also covered by the Fermi satellite, which reported 113 bursts (N. S. Rehan & A. I. Ibrahim 2025). The bursts detected by the Fermi/GBM instrument were on average shorter (log-normal distribution centred at ~ 120 ms) and had lower E_{peak} values (~ 26 keV) than those observed by INTEGRAL, but note that the two studies were based on different samples of bursts that only partially overlapped. These authors found a fluence distribution with $\beta = 1.2 \pm 0.2$ for the October 2022 bursts, steeper than what observed with Fermi/GBM in the other activity periods of SGR 1935+2154, and consistent within the errors with the value we found ($\beta = 0.92 \pm 0.10$).

Our spectral results for the April 2020 burst with associated FRB-like radio emission (burst n. 1118 in our sample, see Fig. 5) agree with those reported in the previous analysis of these data (S. Mereghetti et al. 2020), when one accounts for the different energy ranges of the reported fluxes and the slightly different integration times. In particular, we confirm that the time averaged peak energy was greater than that of bursts of similar fluence (Fig. 4), and that the spectrum hardened with time with E_{peak} evolving from ~ 20 to ~ 100 keV (Fig. 5). The peculiar spectral properties of this bursts were seen also in the data obtained with the Insight-HXMT satellite over the broad energy range of 1–250

keV (C. K. Li et al. 2021) and with Konus-Wind (A. Ridnaia et al. 2021). Several authors speculated that this is related to the unique radio burst emitted during this event (C. D. Bochenek et al. 2020; CHIME/FRB Collaboration et al. 2020), although a clear interpretation of such a connection is still a matter of debate (see, e.g., K. Ioka 2020; C. K. Li et al. 2021; Y. Wu et al. 2025).

Radio bursts from SGR 1935+2154 were detected also on 2020 April 30 (C. F. Zhang et al. 2020), on 2020 September 2 (R. Alexander & V. Fedorova 2020), on 2020 October 8 (D. Good & Chime/FRB Collaboration 2020; U. Giri et al. 2023), on 2022 October 14 and 21 (Y. Maan et al. 2022; F. A. Dong & Chime/FRB Collaboration 2022), and on 2022 December 1 (U. Giri et al. 2023), but unfortunately they were not covered by INTEGRAL data.

Table 7. Parameters of time-resolved spectral analysis of the selected bursts.

Segments were simultaneously fitted with tied alpha.

No	T _{start} ^a	T _{stop} ^a	α	Flux	
				E _{peak} (keV)	(10 ⁻⁷ erg cm ⁻² s ⁻¹)
193	0.000	0.808	0.8 ^{+0.6} -0.3	32.4 ^{+1.5} -0.6	16.4 ± 0.6
	0.000	0.037	2.3 ^{+0.3} -0.9	31.5 ^{+2.7} -3.0	7.4 ^{+1.1} -0.9
	0.047	0.066	...	32.6 ^{+1.3} -1.8	29.4 ^{+2.3} -2.2
	0.066	0.086	...	39.6 ^{+1.4} -1.6	37.9 ^{+2.6} -2.4
	0.086	0.120	...	34.0 ^{+1.2} -1.5	33.2 ^{+2.2} -2.1
	0.229	0.365	...	31.9 ^{+1.8} -2.1	19.8 ^{+2.0} -1.8
	0.429	0.568	...	27.5 ^{+1.5} -2.0	12.7 ^{+1.4} -1.3
	0.624	0.704	...	30.3 ^{+2.3} -2.9	9.0 ^{+1.2} -1.1
	0.760	0.808	...	47.8 ^{+6.7} -7.6	1.6 ^{+0.4} -0.3
	1118	0.000	0.728	-1.1 ± 0.5	66.4 ^{+11.4} -7.7
1244	0.000	0.192	-1.1 ^{+0.4} -0.6	21.6 ^{+4.3} -9.3	1.5 ^{+0.3} -0.2
	0.192	0.255	...	56.5 ^{+12.6} -15.9	13.3 ^{+1.3} -1.2
	0.255	0.300	...	70.5 ^{+12.9} -17.2	29.5 ^{+2.2} -2.0
	0.300	0.338	...	84.7 ^{+19.1} -45.6	20.2 ^{+1.8} -1.7
	0.338	0.728	...	114.0 ^{+40.0} -297.7	2.5 ^{+0.3} -0.2
	1260	0.000	0.616	0.2 ^{+1.1} -0.7	30.1 ± 4.9
	0.000	0.198	0.9 ^{+0.6} -1.0	60.2 ^{+7.3} -8.5	1.8 ^{+0.3} -0.2
	0.198	0.262	...	32.3 ^{+3.8} -4.7	8.3 ^{+0.9} -0.8
	0.262	0.292	...	33.7 ^{+2.9} -3.5	37.9 ^{+2.4} -2.3
	0.292	0.322	...	42.3 ^{+2.8} -3.3	45.1 ^{+2.8} -2.6
1260	0.322	0.352	...	37.4 ^{+3.0} -3.6	38.3 ^{+2.4} -2.3
	0.352	0.382	...	34.4 ^{+2.9} -3.3	37.8 ^{+2.3} -2.2
	0.465	0.616	...	34.5 ^{+3.2} -4.0	16.9 ^{+1.3} -1.2
	0.000	1.853	0.2 ^{+0.8} -0.7	37.1 ^{+3.3} -5.0	3.7 ± 0.1
	0.000	0.523	1.8 ^{+0.5} -0.8	64.5 ^{+16.2} -30.1	0.4 ± 0.1
	0.523	1.089	...	55.0 ^{+6.2} -7.2	1.0 ± 0.1
	1.089	1.377	...	46.8 ^{+4.6} -5.0	1.7 ± 0.2
	1.377	1.458	...	36.1 ^{+3.1} -3.5	5.7 ^{+0.6} -0.5
	1.458	1.490	...	45.2 ^{+2.0} -2.3	48.2 ^{+2.6} -2.5
	1.490	1.522	...	47.8 ^{+2.0} -2.2	50.9 ^{+2.8} -2.7

Table 7 continued on next page

Table 7 (continued)

No	T_{start}^a	T_{stop}^a	α	E_{peak}	Flux
				(keV)	$(10^{-7} \text{erg cm}^{-2} \text{s}^{-1})$
	1.522	1.554	...	$44.7^{+2.0}_{-2.2}$	$47.8^{+2.6}_{-2.5}$
	1.567	1.654	...	$43.1^{+2.9}_{-3.4}$	$30.0^{+2.6}_{-2.4}$
	1.783	1.853	...	$52.0^{+6.8}_{-7.9}$	$3.1^{+0.6}_{-0.5}$
1310	0.000	0.281	$0.5^{+1.5}_{-1.0}$	$33.7^{+4.9}_{-6.7}$	6.7 ± 0.3
	0.032	0.059	$4.3^{+1.3}_{-1.7}$	$30.6^{+3.7}_{-3.8}$	$4.8^{+0.8}_{-0.7}$
	0.059	0.085	...	$45.3^{+1.7}_{-1.6}$	$38.1^{+2.3}_{-2.1}$
	0.085	0.111	...	46.3 ± 1.9	$28.6^{+2.0}_{-1.9}$
	0.111	0.281	...	$40.1^{+3.7}_{-3.8}$	1.1 ± 0.2

^aTime in seconds since T_{start} as defined in Table 2.

6. CONCLUSIONS

We have carried out a comprehensive search for short bursts in data of the INTEGRAL IBIS instrument, taken in the period from end of February 2003 to October 2024. The search for bursts in the light curves resulted more than 75,000 candidates. Exploiting the ISGRI imaging capability, we could verify the nature of each of them, which was especially important in the crowded region of Galactic Centre where multiple sources are present in the FOV. This led to a final sample of 1349 confirmed bursts from 21 different sources.

The total exposure across all sources amounted to 1136.8 Ms, with individual exposures ranging from ~ 8 Ms for CXO0100–7211 in the Small Magellanic Cloud to nearly 68 Ms for SGRJ1745–2900, located close to the Galactic center that was extensively observed by INTEGRAL. Nine magnetars were observed for more than 50 Ms; however, only one of them, SGR 1806–20, produced a significant number of bursts. In contrast, the two next most active sources in our sample, SGR 1935+2154 and 1E 1547–5408, were observed for only ~ 33 Ms and ~ 27 Ms, respectively. This is not surprising as typically most of the magnetar bursts are produced during outbursts lasting weeks to months, and many sources were either not active during the INTEGRAL observation periods or the phases of intense activity were missed by INTEGRAL. For example, this is the case of SGR 1935+2154 that underwent multiple outbursts since 2015 (e.g., [L. Lin et al. 2020a,b](#); [A. Borghese et al. 2020](#); [A. Y. Ibrahim et al. 2024](#); [N. S. Rehan & A. I. Ibrahim 2025](#)), but was observed by INTEGRAL mostly during the 2022 October activity period.

Similar to previous works, we found that the distribution of burst durations are well described by log-normal functions centred around ~ 0.1 s and that the burst fluences follow power-law distributions with integral slopes $\beta \sim 0.7$ –1. The power law distributions of burst energies suggest that a self-organized critical system might be at the bases of the sudden energy release of the bursts ([B. Cheng et al. 1996](#); [M. J. Aschwanden et al. 2016](#)).

We could perform a spectroscopic analysis only for the bursts with sufficient statistics (about 40% of our sample). Most of the time averaged spectra were adequately fit with a simple power law. This resulted from the relatively limited energy range over which the bursts were detected (which also decreased with time due to the rising lower energy threshold of ISGRI) coupled to the large statistical errors. In fact, in the bursts spectra with good counting statistics, an exponential cut-off was clearly required at high energies. In these cases, the best fit peak energies E_{peak} derived with an exponentially cut-off power law model were typically in the range ~ 20 –60 keV for SGR 1806–20 and SGR 1935+2154 and slightly higher for 1E 1547–5408 (~ 35 –100 keV). A time resolved spectral analysis for 21 bursts with high fluence, did not provide evidence for strong spectral evolution, with the notable exception of the SGR 1935+2154 burst with associated FRB-like radio emission.

We found a negative correlation between E_{peak} and fluence for SGR 1806–20. This confirms the reported trends of spectral softening with increasing flux ([D. Götz et al. 2006](#)) and fluence ([E. Gögiş et al. 2001](#)), that were based only on the analysis of hardness ratios. Negative correlations between E_{peak} and fluence have been seen for other magnetars, including 1E 1547–5408 and SGR 1935+2154, also with some evidence for a positive correlation at the highest fluences ([A. J. van der Horst et al. 2012](#); [A. C. Collazzi et al. 2015](#); [L. Lin et al. 2020b, 2011](#)). Our smaller samples of bursts

from the two latter sources do not provide significant evidence for correlations, when measurement errors are properly taken into account.

ACKNOWLEDGEMENTS

We thank D. Götz, C. Ferrigno and Ph. Laurent for their valuable support and help with the data analysis and the anonymous referee for her/his constructive comments. We acknowledge financial support from INAF through the Magnetars Large Program Grant and from the Italian Space Agency through the “INTEGRAL ASI-INAF” agreement 2019-35-HH.0. This work is based on data obtained with INTEGRAL, an ESA mission with instruments and science data centres funded by ESA member states, and with the participation of the Russian Federation and the USA.

Facilities: INTEGRAL(IBIS/ISGRI)

Software: astropy (Astropy Collaboration et al. 2013, 2018, 2022), powerlaw (J. Alstott et al. 2014), SciPy (P. Virtanen et al. 2020)

REFERENCES

Alexander, R., & Fedorova, V. 2020, The Astronomer’s Telegram, 14186, 1

Alstott, J., Bullmore, E., & Plenz, D. 2014, PLoS ONE, 9, e85777, doi: [10.1371/journal.pone.0085777](https://doi.org/10.1371/journal.pone.0085777)

Aptekar, R. L., Frederiks, D. D., Golenetskii, S. V., et al. 2001, ApJS, 137, 227, doi: [10.1086/322530](https://doi.org/10.1086/322530)

Archibald, R. F., Kaspi, V. M., Tendulkar, S. P., & Scholz, P. 2016, ApJL, 829, L21, doi: [10.3847/2041-8205/829/1/L21](https://doi.org/10.3847/2041-8205/829/1/L21)

Arnaud, K. A. 1996, in Astronomical Society of the Pacific Conference Series, Vol. 101, Astronomical Data Analysis Software and Systems V, ed. G. H. Jacoby & J. Barnes, 17

Aschwanden, M. J., Crosby, N. B., Dimitropoulou, M., et al. 2016, SSRv, 198, 47, doi: [10.1007/s11214-014-0054-6](https://doi.org/10.1007/s11214-014-0054-6)

Astropy Collaboration, Robitaille, T. P., Tollerud, E. J., et al. 2013, A&A, 558, A33, doi: [10.1051/0004-6361/201322068](https://doi.org/10.1051/0004-6361/201322068)

Astropy Collaboration, Price-Whelan, A. M., Sipőcz, B. M., et al. 2018, AJ, 156, 123, doi: [10.3847/1538-3881/aabc4f](https://doi.org/10.3847/1538-3881/aabc4f)

Astropy Collaboration, Price-Whelan, A. M., Lim, P. L., et al. 2022, ApJ, 935, 167, doi: [10.3847/1538-4357/ac7c74](https://doi.org/10.3847/1538-4357/ac7c74)

Blumer, H., Safi-Harb, S., McLaughlin, M. A., & Fiore, W. 2021, ApJL, 911, L6, doi: [10.3847/2041-8213/abf11d](https://doi.org/10.3847/2041-8213/abf11d)

Bochenek, C. D., Ravi, V., Belov, K. V., et al. 2020, Nature, 587, 59, doi: [10.1038/s41586-020-2872-x](https://doi.org/10.1038/s41586-020-2872-x)

Borghese, A., Coti Zelati, F., Rea, N., et al. 2020, ApJL, 902, L2, doi: [10.3847/2041-8213/aba82a](https://doi.org/10.3847/2041-8213/aba82a)

Cai, C., Xiong, S.-L., Lin, L., et al. 2022a, ApJS, 260, 25, doi: [10.3847/1538-4365/ac67e4](https://doi.org/10.3847/1538-4365/ac67e4)

Cai, C., Xue, W.-C., Li, C.-K., et al. 2022b, ApJS, 260, 24, doi: [10.3847/1538-4365/ac6172](https://doi.org/10.3847/1538-4365/ac6172)

Camilo, F., Ransom, S. M., Halpern, J. P., & Reynolds, J. 2007, ApJL, 666, L93, doi: [10.1086/521826](https://doi.org/10.1086/521826)

Cheng, B., Epstein, R. I., Guyer, R. A., & Young, A. C. 1996, Nature, 382, 518, doi: [10.1038/382518a0](https://doi.org/10.1038/382518a0)

CHIME/FRB Collaboration, Andersen, B. C., Bandura, K. M., et al. 2020, Nature, 587, 54, doi: [10.1038/s41586-020-2863-y](https://doi.org/10.1038/s41586-020-2863-y)

Clauset, A., Shalizi, C. R., & Newman, M. E. J. 2009, SIAM Review, 51, 661, doi: [10.1137/070710111](https://doi.org/10.1137/070710111)

Collazzi, A. C., Kouveliotou, C., van der Horst, A. J., et al. 2015, ApJS, 218, 11, doi: [10.1088/0067-0049/218/1/11](https://doi.org/10.1088/0067-0049/218/1/11)

Coti Zelati, F., Rea, N., Pons, J. A., Campana, S., & Esposito, P. 2018, MNRAS, 474, 961, doi: [10.1093/mnras/stx2679](https://doi.org/10.1093/mnras/stx2679)

Crawford, D. F., Jauncey, D. L., & Murdoch, H. S. 1970, ApJ, 162, 405, doi: [10.1086/150672](https://doi.org/10.1086/150672)

Curran, P. A. 2014, arXiv e-prints, arXiv:1411.3816, doi: [10.48550/arXiv.1411.3816](https://doi.org/10.48550/arXiv.1411.3816)

Dong, F. A., & Chime/FRB Collaboration. 2022, The Astronomer’s Telegram, 15681, 1

Gavriil, F. P., Gonzalez, M. E., Gotthelf, E. V., et al. 2008, Science, 319, 1802, doi: [10.1126/science.1153465](https://doi.org/10.1126/science.1153465)

Gavriil, F. P., Kaspi, V. M., & Woods, P. M. 2004, ApJ, 607, 959, doi: [10.1086/383564](https://doi.org/10.1086/383564)

Gelfand, J. D., & Gaensler, B. M. 2007, ApJ, 667, 1111, doi: [10.1086/520526](https://doi.org/10.1086/520526)

Gill, R., & Heyl, J. S. 2010, MNRAS, 407, 1926, doi: [10.1111/j.1365-2966.2010.17038.x](https://doi.org/10.1111/j.1365-2966.2010.17038.x)

Giri, U., Andersen, B. C., Chawla, P., et al. 2023, arXiv e-prints, arXiv:2310.16932, doi: [10.48550/arXiv.2310.16932](https://doi.org/10.48550/arXiv.2310.16932)

Goldwurm, A., David, P., Foschini, L., et al. 2003, A&A, 411, L223, doi: [10.1051/0004-6361:20031395](https://doi.org/10.1051/0004-6361:20031395)

Good, D., & Chime/Frb Collaboration. 2020, The Astronomer's Telegram, 14074, 1

Gordon, C., & Arnaud, K. 2021, PyXspec: Python interface to XSPEC spectral-fitting program., Astrophysics Source Code Library, record ascl:2101.014

Götz, D., Mereghetti, S., Molkov, S., et al. 2006, A&A, 445, 313, doi: [10.1051/0004-6361:20053648](https://doi.org/10.1051/0004-6361:20053648)

Göögüs, E., Lin, L., Kaneko, Y., et al. 2016, ApJL, 829, L25, doi: [10.3847/2041-8205/829/2/L25](https://doi.org/10.3847/2041-8205/829/2/L25)

Göögüs, E., Woods, P. M., Kouveliotou, C., et al. 1999, ApJL, 526, L93, doi: [10.1086/312380](https://doi.org/10.1086/312380)

Göögüs, E., Kouveliotou, C., Woods, P. M., et al. 2001, ApJ, 558, 228, doi: [10.1086/322463](https://doi.org/10.1086/322463)

Göögüs, E., Woods, P. M., Kouveliotou, C., et al. 2000, ApJL, 532, L121, doi: [10.1086/312583](https://doi.org/10.1086/312583)

Gros, A., Goldwurm, A., Soldi, S., et al. 2013, arXiv e-prints, arXiv:1302.6915, doi: [10.48550/arXiv.1302.6915](https://doi.org/10.48550/arXiv.1302.6915)

Hajdas, W., Bühler, P., Eggel, C., et al. 2003, A&A, 411, L43, doi: [10.1051/0004-6361:20031251](https://doi.org/10.1051/0004-6361:20031251)

Hurley, K. J., McBreen, B., Rabbette, M., & Steel, S. 1994, A&A, 288, L49

Ibrahim, A. Y., Borghese, A., Coti Zelati, F., et al. 2024, ApJ, 965, 87, doi: [10.3847/1538-4357/ad293b](https://doi.org/10.3847/1538-4357/ad293b)

Ioka, K. 2020, ApJL, 904, L15, doi: [10.3847/2041-8213/abc6a3](https://doi.org/10.3847/2041-8213/abc6a3)

Kaneko, Y., Göögüs, E., Baring, M. G., et al. 2021, ApJL, 916, L7, doi: [10.3847/2041-8213/ac0fe7](https://doi.org/10.3847/2041-8213/ac0fe7)

Kaspi, V. M., & Beloborodov, A. M. 2017, ARA&A, 55, 261, doi: [10.1146/annurev-astro-081915-023329](https://doi.org/10.1146/annurev-astro-081915-023329)

Kouveliotou, C., Fishman, G. J., Meegan, C. A., et al. 1994, Nature, 368, 125, doi: [10.1038/368125a0](https://doi.org/10.1038/368125a0)

Kouveliotou, C., Dieters, S., Strohmayer, T., et al. 1998, Nature, 393, 235, doi: [10.1038/30410](https://doi.org/10.1038/30410)

Kuulkers, E., Ferrigno, C., Kretschmar, P., et al. 2021, NewAR, 93, 101629, doi: [10.1016/j.newar.2021.101629](https://doi.org/10.1016/j.newar.2021.101629)

Labanti, C., Di Cocco, G., Ferro, G., et al. 2003, A&A, 411, L149, doi: [10.1051/0004-6361:20031356](https://doi.org/10.1051/0004-6361:20031356)

Laros, J. G., Fenimore, E. E., Klebesadel, R. W., et al. 1987, ApJL, 320, L111, doi: [10.1086/184985](https://doi.org/10.1086/184985)

Lebrun, F. 2005, IEEE Transactions on Nuclear Science, 52, 3119, doi: [10.1109/TNS.2005.862920](https://doi.org/10.1109/TNS.2005.862920)

Lebrun, F., Leray, J. P., Lavocat, P., et al. 2003, A&A, 411, L141, doi: [10.1051/0004-6361:20031367](https://doi.org/10.1051/0004-6361:20031367)

Li, C. K., Lin, L., Xiong, S. L., et al. 2021, Nature Astronomy, 5, 378, doi: [10.1038/s41550-021-01302-6](https://doi.org/10.1038/s41550-021-01302-6)

Lin, L., Göögüs, E., Roberts, O. J., et al. 2020a, ApJL, 902, L43, doi: [10.3847/2041-8213/abbebe](https://doi.org/10.3847/2041-8213/abbebe)

Lin, L., Göögüs, E., Roberts, O. J., et al. 2020b, ApJ, 893, 156, doi: [10.3847/1538-4357/ab818f](https://doi.org/10.3847/1538-4357/ab818f)

Lin, L., Kouveliotou, C., Baring, M. G., et al. 2011, ApJ, 739, 87, doi: [10.1088/0004-637X/739/2/87](https://doi.org/10.1088/0004-637X/739/2/87)

Lin, L., Göögüs, E., Baring, M. G., et al. 2012, ApJ, 756, 54, doi: [10.1088/0004-637X/756/1/54](https://doi.org/10.1088/0004-637X/756/1/54)

Lund, N., Budtz-Jørgensen, C., Westergaard, N. J., et al. 2003, A&A, 411, L231, doi: [10.1051/0004-6361:20031358](https://doi.org/10.1051/0004-6361:20031358)

Lyutikov, M. 2003, MNRAS, 339, 623, doi: [10.1046/j.1365-8711.2003.06141.x](https://doi.org/10.1046/j.1365-8711.2003.06141.x)

Maan, Y., Leeuwen, J. v., Straal, S., & Pastor-Marazuela, I. 2022, The Astronomer's Telegram, 15697, 1

Mazets, E. P., Cline, T. L., Aptekar', R. L., et al. 1999, Astronomy Letters, 25, 628, doi: [10.48550/arXiv.astro-ph/9905195](https://doi.org/10.48550/arXiv.astro-ph/9905195)

Mazets, E. P., & Golenetskii, S. V. 1981, Ap&SS, 75, 47, doi: [10.1007/BF00651384](https://doi.org/10.1007/BF00651384)

Mereghetti, S., Esposito, P., Tiengo, A., et al. 2012, A&A, 546, A30, doi: [10.1051/0004-6361/201219907](https://doi.org/10.1051/0004-6361/201219907)

Mereghetti, S., Götz, D., Borkowski, J., Walter, R., & Pedersen, H. 2003, A&A, 411, L291, doi: [10.1051/0004-6361:20031289](https://doi.org/10.1051/0004-6361:20031289)

Mereghetti, S., Pons, J. A., & Melatos, A. 2015, SSRv, 191, 315, doi: [10.1007/s11214-015-0146-y](https://doi.org/10.1007/s11214-015-0146-y)

Mereghetti, S., Tiengo, A., Esposito, P., et al. 2005, ApJ, 628, 938, doi: [10.1086/430943](https://doi.org/10.1086/430943)

Mereghetti, S., Götz, D., Weidenspointner, G., et al. 2009, ApJL, 696, L74, doi: [10.1088/0004-637X/696/1/L74](https://doi.org/10.1088/0004-637X/696/1/L74)

Mereghetti, S., Savchenko, V., Ferrigno, C., et al. 2020, ApJL, 898, L29, doi: [10.3847/2041-8213/aba2cf](https://doi.org/10.3847/2041-8213/aba2cf)

Palmer, D. M., Barthelmy, S. D., Cummings, J. R., et al. 2015, GRB Coordinates Network, 18634, 1

Parfrey, K., Beloborodov, A. M., & Hui, L. 2013, ApJ, 774, 92, doi: [10.1088/0004-637X/774/2/92](https://doi.org/10.1088/0004-637X/774/2/92)

Prieskorn, Z., & Kaaret, P. 2012, ApJ, 755, 1, doi: [10.1088/0004-637X/755/1/1](https://doi.org/10.1088/0004-637X/755/1/1)

Rehan, N. S., & Ibrahim, A. I. 2025, ApJS, 276, 60, doi: [10.3847/1538-4365/ad95f9](https://doi.org/10.3847/1538-4365/ad95f9)

Ridnaia, A., Svinkin, D., Frederiks, D., et al. 2021, Nature Astronomy, 5, 372, doi: [10.1038/s41550-020-01265-0](https://doi.org/10.1038/s41550-020-01265-0)

Sathyaprakash, R., Rea, N., Coti Zelati, F., et al. 2024, ApJ, 976, 56, doi: [10.3847/1538-4357/ad8226](https://doi.org/10.3847/1538-4357/ad8226)

Savchenko, V., Neronov, A., Beckmann, V., Produit, N., & Walter, R. 2010, A&A, 510, A77, doi: [10.1051/0004-6361/200911988](https://doi.org/10.1051/0004-6361/200911988)

Scargle, J. D. 1998, ApJ, 504, 405, doi: [10.1086/306064](https://doi.org/10.1086/306064)

Scargle, J. D., Norris, J. P., Jackson, B., & Chiang, J. 2013, ApJ, 764, 167, doi: [10.1088/0004-637X/764/2/167](https://doi.org/10.1088/0004-637X/764/2/167)

Scholz, P., & Kaspi, V. M. 2011, ApJ, 739, 94, doi: [10.1088/0004-637X/739/2/94](https://doi.org/10.1088/0004-637X/739/2/94)

Thompson, C., & Duncan, R. C. 1995, MNRAS, 275, 255, doi: [10.1093/mnras/275.2.255](https://doi.org/10.1093/mnras/275.2.255)

Thompson, C., & Duncan, R. C. 1996, *ApJ*, 473, 322, doi: [10.1086/178147](https://doi.org/10.1086/178147)

Thompson, C., & Duncan, R. C. 2001, *ApJ*, 561, 980, doi: [10.1086/323256](https://doi.org/10.1086/323256)

Ubertini, P., Lebrun, F., Di Cocco, G., et al. 2003, *A&A*, 411, L131, doi: [10.1051/0004-6361:20031224](https://doi.org/10.1051/0004-6361:20031224)

Ulmer, A., Fenimore, E. E., Epstein, R. I., et al. 1993, *ApJ*, 418, 395, doi: [10.1086/173399](https://doi.org/10.1086/173399)

van der Horst, A. J., Kouveliotou, C., Gorgone, N. M., et al. 2012, *ApJ*, 749, 122, doi: [10.1088/0004-637X/749/2/122](https://doi.org/10.1088/0004-637X/749/2/122)

Vedrenne, G., Roques, J. P., Schönfelder, V., et al. 2003, *A&A*, 411, L63, doi: [10.1051/0004-6361:20031482](https://doi.org/10.1051/0004-6361:20031482)

Virtanen, P., Gommers, R., Oliphant, T. E., et al. 2020, *Nature Methods*, 17, 261, doi: [10.1038/s41592-019-0686-2](https://doi.org/10.1038/s41592-019-0686-2)

von Kienlin, A., Gruber, D., Kouveliotou, C., et al. 2012, *ApJ*, 755, 150, doi: [10.1088/0004-637X/755/2/150](https://doi.org/10.1088/0004-637X/755/2/150)

Wu, Y., Yang, Y.-P., Wang, F.-Y., & Dai, Z.-G. 2025, *ApJ*, 988, 274, doi: [10.3847/1538-4357/ade884](https://doi.org/10.3847/1538-4357/ade884)

Younes, G., Baring, M. G., Kouveliotou, C., et al. 2017, *ApJ*, 851, 17, doi: [10.3847/1538-4357/aa96fd](https://doi.org/10.3847/1538-4357/aa96fd)

Younes, G., Güver, T., Kouveliotou, C., et al. 2020, *ApJL*, 904, L21, doi: [10.3847/2041-8213/abc94c](https://doi.org/10.3847/2041-8213/abc94c)

Zhang, C. F., Jiang, J. C., Men, Y. P., et al. 2020, *The Astronomer's Telegram*, 13699, 1